INTERNATIONAL JOURNAL FOR NUMERICAL METHODS IN FLUIDS
Int. J. Numer. Meth. Fluids 2007; **53**:1381–1397
Published online 10 October 2006 in Wiley InterScience (www.interscience.wiley.com). DOI: 10.1002/fld.1370

A numerical strategy for modelling rotating stall in core compressors

M. Vahdati*, †

Imperial College London, Vibration UTC, MED, London, SW7 2BX, U.K.

SUMMARY

The paper will focus on one specific core-compressor instability, rotating stall, because of the pressing industrial need to improve current design methods. The determination of the blade response during rotating stall is a difficult problem for which there is no reliable procedure. During rotating stall, the blades encounter the stall cells and the excitation depends on the number, size, exact shape and rotational speed of these cells. The long-term aim is to minimize the forced response due to rotating stall excitation by avoiding potential matches between the vibration modes and the rotating stall pattern characteristics. Accurate numerical simulations of core-compressor rotating stall phenomena require the modelling of a large number of bladerows using grids containing several tens of millions of points. The time-accurate unsteady-flow computations may need to be run for several engine revolutions for rotating stall to get initiated and many more before it is fully developed. The difficulty in rotating stall initiation arises from a lack of representation of the triggering disturbances which are inherently present in aeroengines. Since the numerical model represents a symmetric assembly, the only random mechanism for rotating stall initiation is provided by numerical round-off errors. In this work, rotating stall is initiated by introducing a small amount of geometric mistuning to the rotor blades. Another major obstacle in modelling flows near stall is the specification of appropriate upstream and downstream boundary conditions. Obtaining reliable boundary conditions for such flows can be very difficult. In the present study, the low-pressure compression (LPC) domain is placed upstream of the core compressor. With such an approach, only far field atmospheric boundary conditions are specified which are obtained from aircraft speed and altitude. A chocked variable-area nozzle, placed after the last compressor bladerow in the model, is used to impose boundary conditions downstream. Such an approach is representative of modelling an engine.

Using a 3D viscous time-accurate flow representation, the front bladerows of a core compressor were modelled in a whole-annulus fashion whereas the rest of bladerows are modelled in a single-passage fashion. The rotating stall behaviour at two different compressor operating points was studied by considering two different variable-vane scheduling conditions for which experimental data were available. Using a model with nine whole-assembly models, the unsteady-flow calculations were conducted on 32-CPUs of a parallel cluster, typical run times being around 3–4 weeks for a grid with about 60 million points. The simulations were conducted over several engine rotations. As observed on the actual development engine, there was no

*Correspondence to: M. Vahdati, Imperial College London, Vibration UTC, MED, London, SW7 2BX, U.K.
†E-mail: m.vahdati@ic.ac.uk

Contract/grant sponsor: Rolls-Royce plc.

rotating stall for the first scheduling condition while mal-scheduling of the stator vanes created a 12-band rotating stall which excited the 1st flap mode. Copyright © 2006 John Wiley & Sons, Ltd.

Received 28 November 2005; Revised 17 July 2006; Accepted 6 August 2006

KEY WORDS: aeroelasticity; core compressor; rotating stall

1. INTRODUCTION

Unsteady turbulent high-speed compressible flows often give rise to complex aeroelasticity phenomena by influencing the dynamic behaviour of structures on which they act. Under certain conditions, the energy transfer from the fluid to the structure can cause excessive vibration levels and structural integrity may be compromized. The problem is particularly severe for gas turbines where virtually all bladerows are susceptible to aeroelasticity effects either by inherent self-induced motion (flutter) or by response to aerodynamic flow distortions and blade wakes (forced response). The most complex and the least understood aeroelasticity phenomena occur in multi-stage core compressors, the subject of this paper, because of their wide operating envelope. The performance of an axial-flow compressor is often summarized in the form of a pressure-rise versus mass flow characteristic map (Figure 1), representing nominally steady and axisymmetric flow operation. At a given shaft speed, the operating zone is bounded by choke at high mass flow/low pressure (point D), and by surge at low mass flow/high pressure (point A). During engine development programmes, costly structural failures are known to occur because of a mixture of aeroelastic instabilities such as acoustic resonance, flutter, forced response, rotating stall, surge, etc. Apart from surge which is a global event, most such phenomena are believed to be caused by at least one bladerow undergoing severe stall, but the overall compressor still managing to function because of the overall pressure ratio. Rotating stall is a disturbance that is *local* to the compressor bladerows

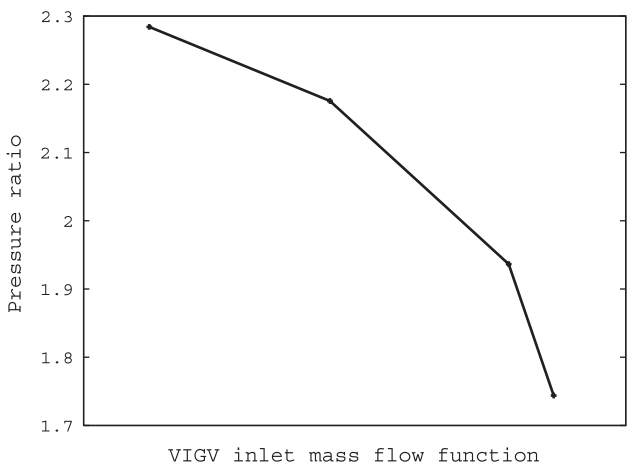

Figure 1. Typical compressor performance curve.

DOI: 10.1002/fld

which is characterized by a circumferential non-uniform flow deficit, with one or more stall cells propagating around the compressor circumference at a fraction of the shaft speed, typically between 20 and 60%. In fully developed rotating stall, the overall flow through the compressor is constant in time, with the stall cells redistributing the flow around the annulus. The numerical modelling of such a situation is a formidable challenge as the analysis must be able to represent accurately not only the aerodynamic and structural properties of a large number of bladerows, but also the interactions through these.

Since the avoidance of stall and surge is a major design consideration, a considerable amount of research effort has been devoted to the understanding of the physical mechanisms that give rise to such instabilities. After the initial inception stage, it is not clear which conditions will cause surge or rotating stall, though a simplified non-dimensional parameter, based on basic geometry, the mean flow speed and the speed of sound, has been proposed by Greitzner [1] who provided a means of assessing how design changes were likely to affect the stall/surge behaviour of a particular compressor. However, in the general case, there are no rules to determine the speed of rotating stall, its circumferential and radial extent as well as the number of rotating cells. So far, due to modelling difficulties, much of the stall and surge research has been experimental [2, 3], or based on simplified models [4, 5], though numerical simulations with simplified or partial geometries are beginning to emerge [6, 7]. There is some more recent work by Chen and his colleagues [8] involving numerical simulations for stall prediction and prevention.

Unlike other instabilities of aeroelastic origin, core-compressor rotating stall behaviour needs to be simulated not only at the onset, but also during the event itself. Such a requirement arises from the need to avoid a match between the number and speed of rotating stall cells and the assembly resonances. From an industrial perspective, it is important to understand the factors which influence changes in stall characteristics as it may result in moving from a safe operating regime to one which causes rotor blade failure. These effects are normally assessed by engine strain gauge tests which are used to map out rotating stall boundaries. However, due to the high cost of these tests and the limited scope for varying engine configuration and operation, the objective of this work is to develop a predictive capability which will minimize rig and engine testing by means of advanced simulations that will cover the flight envelope in an efficient manner.

2. OVERVIEW OF THE FORCED RESPONSE METHODOLOGY

2.1. Flow model

The unsteady, compressible Reynolds-averaged Navier–Stokes equations for a 3D bladerow can be cast in terms of absolute velocity $\mathbf{u}$ but solved in a relative reference frame rotating with angular velocity $\boldsymbol{\omega}$. This system of equations, written in an arbitrary Eulerian–Lagrangian conservative form for a control volume Ω with boundary Γ, takes the form

$$\frac{\mathrm{d}}{\mathrm{d}t}\int_{\Omega}\mathbf{U}\,\mathrm{d}\Omega+\oint_{\partial\Omega}\left(\mathbf{F}-\frac{1}{\mathrm{Re}}\mathbf{G}\right)\cdot\mathbf{n}\,\mathrm{d}\Gamma=\int_{\Omega}\mathbf{S}\,\mathrm{d}\Omega \tag{1}$$

where $\mathbf{n}$ represents the outward unit vector of the control volume boundary Γ. The viscous term $\mathbf{G}$ on the left-hand side of (1) has been scaled by the reference Reynolds number for

DOI: 10.1002/fld

non-dimensionalization purposes. The solution vector **U** of conservative variables is given by

$$\mathbf{U}=\begin{bmatrix}\rho\\ \rho u_i\\ \rho\varepsilon\end{bmatrix} \tag{2}$$

The inviscid flux vector **F** can be written as

$$\mathbf{F}=\begin{bmatrix}\rho(u_i-w_i)\\ \rho u_i(u_i-w_i)+p\delta_{ij}\\ \rho E(u_i-w_i)+pu_i\end{bmatrix} \tag{3}$$

where δ_{ij} is the Kronecker delta, u_i and w_i are the absolute and the grid velocities, respectively. The pressure p and the total enthalpy h are related to density ρ by two perfect gas equations

$$p=(\gamma-1)\rho\left(\varepsilon-\frac{|\mathbf{u}^2|}{2}\right),\quad h=\varepsilon+\frac{p}{\rho} \tag{4}$$

where γ is the constant specific heat ratio. The viscous flux vector **G** can be written as

$$\mathbf{G}=\begin{bmatrix}0\\ \sigma_{ij}\\ u_k\sigma_{ik}+\dfrac{\gamma}{\gamma+1}\left(\dfrac{\mu_l}{\mathrm{Pr}_l}+\dfrac{\mu_t}{\mathrm{Pr}_t}\right)\partial T/\partial x_i\end{bmatrix} \tag{5}$$

where μ_l represents the molecular viscosity given by the Sutherland's formula, μ_t denotes the turbulent eddy viscosity, which must be determined using a suitable turbulence model. The model proposed by Spalart and Allmaras [9] was adopted here. The laminar Prandtl number Pr_l is taken as 0.7 for air while the turbulent Prandtl number Pr_t is taken as 0.9. The viscous stress tensor σ_{ij} is expressed using the eddy viscosity concept which assumes that, in analogy with viscous stresses in laminar flows, the turbulent stresses are proportional to mean velocity gradients:

$$\sigma_{ij}=(\mu_l+\mu_t)\left(\frac{\partial u_i}{\partial x_j}+\frac{\partial u_j}{\partial x_i}\right)+\lambda\delta_{ij}(\nabla\cdot\mathbf{u}) \tag{6}$$

The value of λ is given by the Stokes relationship $\lambda=-2/3(\mu_l+\mu_t)$. Vector **S**, which contains the terms due to the rotation of the co-ordinate system, can explicitly be written as

$$\mathbf{S}=\begin{bmatrix}0\\ \rho\omega u_2\\ \rho\omega u_3\end{bmatrix} \tag{7}$$

Equation (1) is discretized on unstructured mixed-element grids via a finite volume method, the details of which are given by Sayma *et al.* [10]. The resulting solver is a cell vertex scheme.

DOI: 10.1002/fld

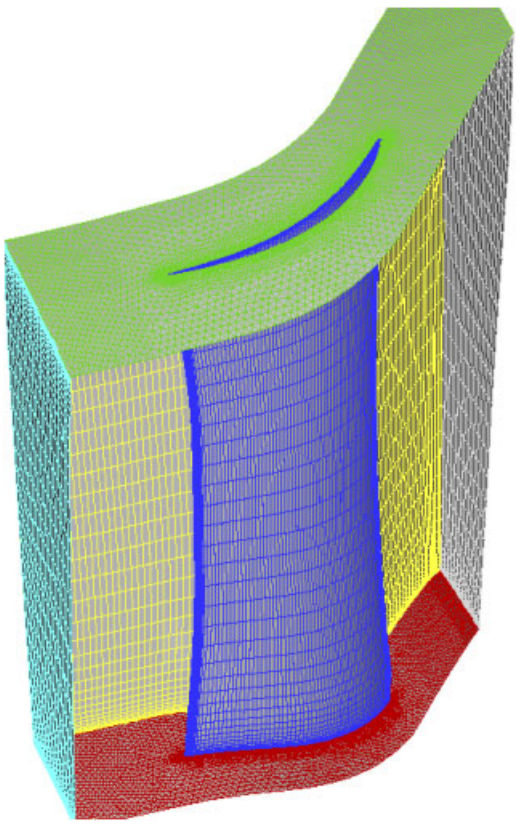

Figure 2. Typical view of the grid used.

As described by Sbardella *et al.* [11], the blades are discretized using a semi-structured mesh which consists of brick elements in the boundary layer and triangular prisms further away in the blade passage, i.e. the grid is only unstructured in a blade to blade plane. Typical view of such grids is shown in Figure 2. To achieve further computational efficiency, the mesh is characterized via an edge-based data structure, i.e. the grid is presented to the solver as a set of node pairs connected by edges, a feature that allows the solver to have a unified data structure. Furthermore, the edge-based formulation has the advantage of computing and storing the edge weights prior to the main unsteady-flow calculation, hence reducing the CPU effort. The central differencing scheme is stabilized using a mixture of second- and fourth-order matrix artificial dissipation. In addition, a pressure switch, which guarantees that the scheme is total variation diminishing (TVD) and reverts to a first-order Roe scheme in the vicinity of discontinuities, is used for numerical robustness. The resulting semi-discrete system of equations is advanced in time using a point-implicit scheme with Jacobi iterations and dual time stepping. Such an approach allows relatively large time steps for the external Newton iteration. For steady-state calculations, solution acceleration techniques, such as residual smoothing and local time stepping are employed. For unsteady computations, an outer Newton iteration procedure is used where the time steps are dictated by the physical restraints

DOI: 10.1002/fld

and fixed through the solution domain. Within the Newton iteration, the solution is advanced to convergence using the traditional acceleration techniques described previously.

The relative motion between the stator and the rotor blades can be modelled using one of the following two types of interface boundaries.

Mixing planes. These boundaries are used to provide an interface between bladerows which are represented as single passages. Since, there is no one-to-one correspondence between the rotor and stator bladerows, the information can only be exchanged in an average sense. In the approach taken here, a circumferential mass averaging of the flow variables is performed at each radial height on both sides of the mixing plane. The flow variables at the rotor side are imposed as boundary condition for stator domain, and the variables at the stator side are prescribed as boundary condition for the rotor domain. Mixing planes are typically used in steady-state flow calculations, especially for multi-stage core compressors. Due to the averaging process, they do not allow the propagation of circumferential waves, and hence they are not suitable for simulating unsteady-flow phenomena such as forced response and rotating stall. However, they can still be used to capture global unsteadiness characteristics such as whole compressor surge where local unsteadiness, say due to blade interactions, is of secondary interest.

Sliding planes. Such boundaries can be used at both whole-annulus and single-passage bladerow interfaces. They model the bladerow interaction correctly and all waves, axial, radial and circumferential, are propagated without any simplifying assumptions. For sliding planes placed at bladerow boundaries, the solution is updated at the interface by interpolating the variables in the stator computational domain to obtain rotor fluxes, and in the rotor computational domain to obtain the stator fluxes [12, 13]. The fluxes are computed using a characteristic technique, which allows the correct propagation of the information. In other words, flow data are exchanged between the two grids via specially formulated boundary conditions at the interface. Sliding planes are typically used in unsteady-flow computations.

2.2. *Structural model and calculation of the aeroelastic response*

It is implicitly assumed that the vibration amplitude remains within the bounds of linear behaviour. The global aeroelasticity equations of a structural motion can be written as

$$\mathbf{M}\ddot{x} + \mathbf{C}\dot{x} + \mathbf{K}x = \mathbf{p}(\mathbf{t})A\mathbf{n} \tag{8}$$

where **M**, **K**, and **C** are the mass, stiffness and damping matrices, **x** is the displacement vector, **p**(**t**) is a vector of pressures, A being the application area and **n** the normal unit vector on the blade's surface. A standard structural finite element formulation is used to obtain the left-hand side while the flow model above is used to obtain the unsteady forcing of the right-hand side. The free vibration problem can be solved to yield the natural frequencies ω_r and mode shapes $\boldsymbol{\phi}_r$ of the bladed disk assembly in vacuum, r being the mode index. A convenient indicator of the blade response is the modal force, which is a measure of the correlation between the structural mode shape and the unsteady pressure fluctuation, the other two key parameters being the amplitude and frequency of the fluctuation. The modal force represents the strength of the unsteady forcing in a particular mode of vibration and is given by

$$f(x, r) = \tilde{p}(x, r)\eta\phi(x, r) \tag{9}$$

DOI: 10.1002/fld

where ϕ is the mode shape vector and η is the area normal vector. The total modal force is obtained by summing the above over all the points on the blade. In simple terms, the modal force may be considered to be the product of the unsteady pressure and the structural mode shape. It can best be visualized by considering a rigid body motion where the blade is plunging only. In this case, the modal force is equivalent to the unsteady lift on the blade.

The aeroelasticity analysis can be conducted in two different ways, the so-called fully coupled and the uncoupled approaches. In the fully coupled method, the structural mode shapes are interpolated onto the aerodynamic mesh as the two discretization levels between structural and aerodynamic meshes are unlikely to be wholly coincident. To accommodate the structural motion, the fluid mesh is moved at each time step using a network of springs whose compression/extension is prescribed by the mode shape at the blade surface and becomes zero at the far field. The frequency of the motion is dictated by the natural frequency of the corresponding mode. An exchange of boundary conditions takes place at the fluid–structure interface at each time step. The main advantage of the fully coupled method is the automatic inclusion of the aerodynamic damping while the main drawback is the computational overhead arising from the mesh movement. However, unless the change in aerodynamic damping is likely to be important, say in the case of a large blade vibrating at resonance, the forced response analysis can be simplified by considering the unsteady flow and the blade motion separately. Such an uncoupled analysis consists of computing the blade unsteady pressures without any blade movement. The aerodynamic damping may still be obtained from a transient aeroelasticity, or flutter, analysis, and such damping values can be used when calculating the blade's response. A case study comparing the relative accuracy of both approaches is reported by Vahdati *et al.* [14].

A convenient indicator of the blade response is the modal force, which is a measure of the correlation between the structural mode shape and the unsteady pressure fluctuation, the other two key parameters being the amplitude and frequency of the fluctuation. The modal force represents the strength of the unsteady forcing in a particular mode of vibration. In simple terms, the modal force can be thought as the product of the unsteady pressure and the structural mode shape. It can best be visualized by considering a rigid body motion where the blade is plunging only. In this case, the modal force is equivalent to the unsteady lift on the blade.

3. BOUNDARY CONDITIONS

A major difficulty in modelling flows near stall is the specification of appropriate upstream and downstream boundary conditions. The usual method for imposing boundary conditions in a core compressor is to specify total pressure, total temperature and the flow angles at the inlet to the first bladerow and to specify the static pressure at the exit of the last bladerow. However, for flows near stall, obtaining reliable and accurate boundary conditions can be very difficult since the engine is operating very far from its design intent. Moreover, the imposition of time-invariant boundary conditions may not be valid as the flow is unsteady within the compressor. Moreover, under certain conditions, such as surge, the flow will be going out the compressor inlet. Therefore, alternative ways of prescribing the inlet and exit conditions for the core compressor is required.

In approach taken here, the upstream conditions are modelled by placing the low-pressure compressor (LPC) domain upstream of the core compressor (Figure 3). The domain contains the intake, fan, the fan guide vanes (OGV) and the ESS. With such an approach, only far field

DOI: 10.1002/fld

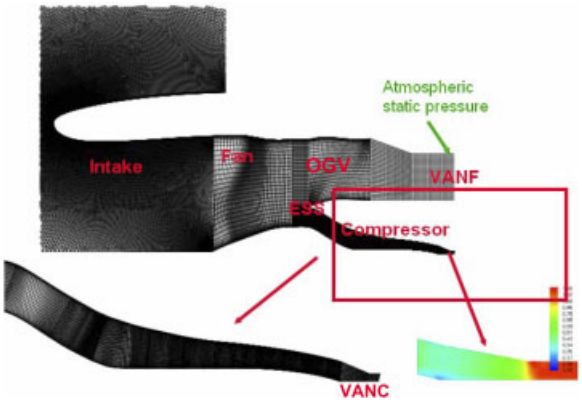

Figure 3. Steady-state flow domain.

atmospheric boundary conditions are specified and the only information required for upstream boundary conditions is the aircraft speed and the ambient conditions at a given altitude. Moreover, with such approach the LP/IP domain interactions which can be very important at off design settings are modelled automatically.

At the exit, it is common engineering practice to specify a fixed static pressure as a downstream boundary condition. It is shown in Reference [15] that rigid boundary conditions, based on imposing given fixed exit pressure distributions, are not suitable for stall studies of a fan blade. For instance, in the case of rotating stall, the downstream exit pressure profiles are neither known nor constant in time. Similarly, at high working lines, the flow becomes genuinely unsteady near the stall boundary, and the imposition of a radially constant exit static pressure is likely to result in numerical instabilities, the so-called 'numerical stall'. As discussed in Reference [15], the situation can be remedied for a single bladerow fan assembly by introducing a downstream variable nozzle, thus allowing the pressure behind the fan to adjust automatically, while the pressure behind the nozzle is fixed. Such an approach makes the computational domain 'less stiff' and provides a powerful natural boundary condition for stall studies. Moreover, since the aim is to simulate, as much as possible, engine and rig tests, nozzle area changes can be used to move to any point on the compressor characteristic. In the present study a similar approach is taken by placing a variable nozzle downstream of the last bladerow of the compressor. The flow in the nozzle is choked, hence the nozzle area change determines the mass flow and the operating point on the core-compressor characteristic and the solution is independent of prescribed boundary condition at the nozzle exit. With such an approach, nothing is fixed at the exit, and hence it is very well suited for a genuinely unsteady flow.

The flow through the engine is controlled by using two downstream variable-area nozzles (Figure 3). The by-pass duct nozzle (VANF), downstream of the fan OGVs, is adjusted to obtain the correct fan operating point and the by-pass ratio. Once this is obtained, this nozzle is kept fixed for the rest of the computations, and hence assuming that the fan operating point remains the same for all the compressor conditions. Atmospheric static pressure is assumed at the exit of the by-pass nozzle. A second variable-area nozzle (VANC) is used down stream of the compressor. The compressor nozzle is gradually closed until the flow approaches stall.

DOI: 10.1002/fld

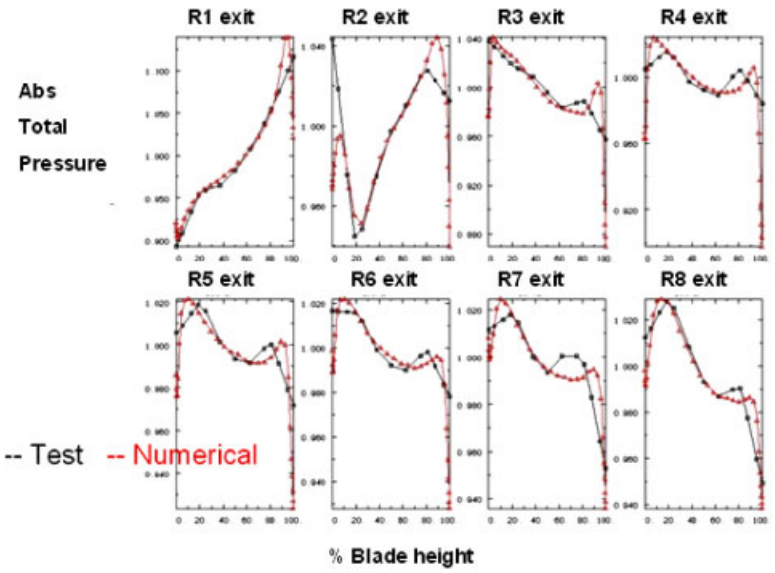

Figure 4. Comparison of computed total pressure at rotors exit planes against test data.

Figure 4 shows the comparison of computed and measured total pressure profiles downstream of rotor blades for an 8-stage compressor near stall (each subfigure corresponds to the stage rotor). The experimental data were obtained from a test rig. It is seen that the proposed methodology can produce reasonably good agreement with measured data for such flows.

4. COMPUTATIONAL DOMAIN

There are very few methods that allow a 3D time-accurate modelling of rotating stall in a core compressor. A whole-assembly analysis of whole compressor is computationally very expensive because of the large number of engine rotations that need to be simulated as well as the number of points required in the model. However, given the computational cost, taking advantage of the circular symmetry, i.e. ignoring potential differences around the annulus, becomes quite critical. However, not all unsteady phenomena can be confined to the symmetry of a single passage. For instance, rotating stall can only be studied with a whole-annulus model. A possible compromise to reduce the computational cost is the use of a hybrid single-passage whole-annulus model. In this approach, the bladerows of interest are modelled in whole-annulus fashion, while the remaining bladerows are represented as single blade passages (Figure 5). The interface boundaries between the whole-annulus bladerows are represented by sliding planes, while the remaining interface boundaries are treated as mixing planes. Depending how the solution develops, any single-passage bladerow can be replaced by a whole-annulus bladerow and *vice versa* during the course of the computations. The approach is best suited for simulating the so-called 'part-span stall' which is confined to a relatively small area of the compressor. The mixing planes transfer the information in an average sense, and hence should be placed a sufficient distance from the regions with significant

DOI: 10.1002/fld

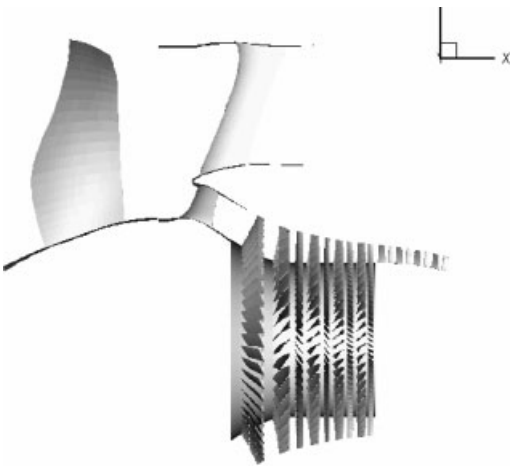

Figure 5. Hybrid single-passage (SP) whole-annulus (WA) model.

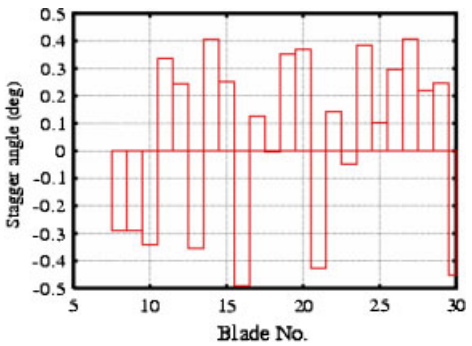

Figure 6. Mistuning pattern used in current study.

circumferential variations. If they are placed too close to such regions they will affect the unsteady aerodynamic loadings.

The other major difficulty is the initiation of rotating stall numerically. The analysis usually starts using an initial solution obtained using one-passage steady-state flow analysis. For instability to be triggered, the flow must be perturbed. If the whole-annulus unsteady-flow analysis is performed for a perfectly symmetric geometry, there is no aerodynamic difference between the passages, the so-called aerodynamic mistuning, rotating stall can only develop, after a perhaps 100 engine revolutions, when rounding-off errors become significant enough to cause a perturbation. For computational efficiency, it is essential to drive the numerical model into rotating stall as quickly as possible. In the approach taken here, rotating stall is initiated by introducing a small amount of aerodynamic mistuning to the blade passages by changing the stagger angle of blades in a random fashion (Figure 6). The amount of mistuning introduced is within the manufacturing and

DOI: 10.1002/fld

assembly tolerances. The aerodynamically mistuned domain is obtained forming a tuned whole-annulus domain from a single-passage grid first. The blades are then moved according to the desired mistuning pattern. The grid movement algorithm described in Reference [14] is used to insure the quality of grid does not degenerate.

5. CASE STUDY

As stated earlier, the objective of the work is to develop a methodology to predict the effects of multi-lobe rotating stall on blade vibration levels. Of particular importance is to link the variable-vane scheduling to the number, size, distribution and speed of rotating stall cells so that the critical modes of vibration can be identified and avoided. The test case chosen is an 8-stage compressor where the first three stator bladerows have variable-angle vanes. Two vane settings, namely nominal and mal-scheduled, were used in the computations because of the availability of experimental data for these two conditions.

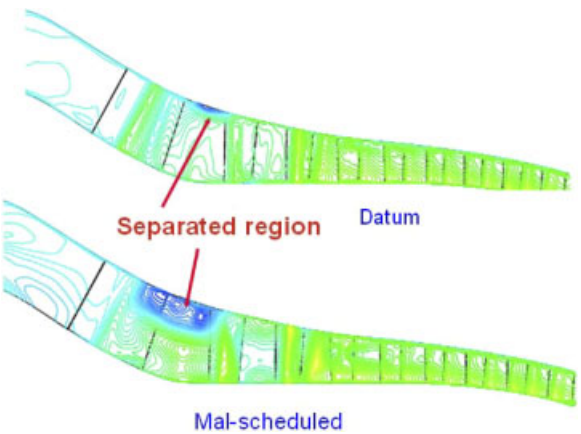

Figure 7. Steady-state axial velocity profiles at mid passage.

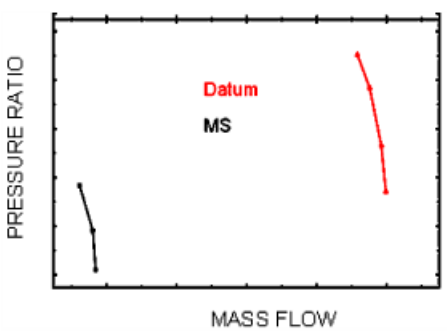

Figure 8. Compressor over all performance.

DOI: 10.1002/fld

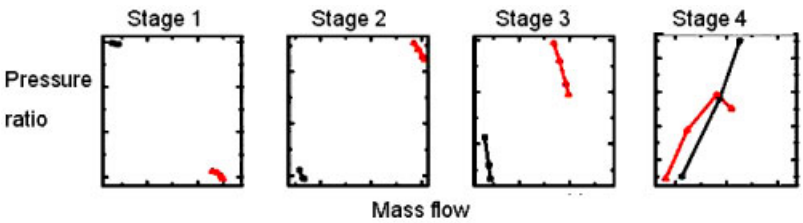

Figure 9. Stage performance for the compressor.

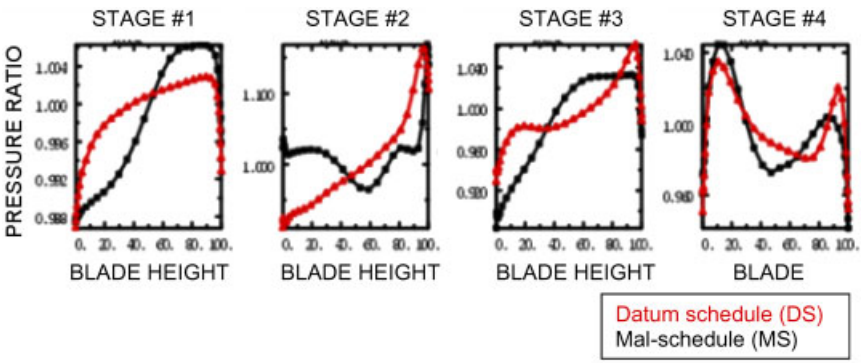

Figure 10. Variations of total pressure at stator inlets.

5.1. Steady-state flow results

In the steady-flow computations, the entire domain is modelled using single passages (Figure 3). A sample view of steady-state flow results obtained for the two VSV conditions are shown in Figures 7–10. The following differences between datum schedule (DS) and mal-schedule (MS) can be observed in the steady-state flow solution.

- The separated flow region on Rotor 1 extends much further radially for the MS case (Figure 7).
- The separated flow region extends into the upstream and down stream bladerows for the MS case.
- Compressor characteristics, such as the overall mass flow, pressure ratio and efficiency, drop significantly for the MS case.
- The Rotor 1 pressure ratio increases but Rotor 2 and Rotor 3 pressure ratios decrease. Hence, Rotor 1 experiences the worst flow conditions under this mal-scheduling condition. The pressure ratio for stages 4 and on wards is not greatly affected.

As can be seen from Figure 10, the inlet profiles to the compressor are significantly different between the two scheduling cases, the compressor having much weaker inlet profiles for the MS case. This indicates that there is a strong interaction between the IP and the LP domains: the massive separation around the Rotor 1 tip affects the flow at the fan root, which in turn affects the

DOI: 10.1002/fld

flow into the core compressor. Therefore, the inclusion of the LP domain is critical for the correct prediction of the onset of rotating stall.

5.2. *Unsteady-flow results*

The first 9 bladerows of the compressor are modelled in a whole-annulus fashion, whereas the rest of the compressor, as well as the LP domain, are modelled using single passages. The computational domain is shown in Figure 5. The total number of grid points is about 60 million. The variation of the static pressure upstream of Rotor 1 after 13 engine rotations is shown in Figure 11. It is seen that the flow looks symmetric for the DS case, i.e. sign of no rotating stall, but a non-symmetric pattern, i.e. rotating stall, develops for the MS case. It should be noted that the same amount of aerodynamic mistuning is used for both vane schedules, and hence the formation of stall cells depends on how the flow solution develops, rather than which aerodynamic mistuning pattern is imposed. The variations of the instantaneous static pressure upstream of Rotor 1 along the circumference at 70 and 90% heights are shown in Figure 12 together with the corresponding Fourier components. A close study of these figures reveals the existence of a 12-band rotating stall for the MS case. Moreover, the figure shows that the rotating stall is much stronger at 70% height. The variations of static pressure upstream of R1 at four different time levels are shown in Figure 13. It is seen that about 13 engine rotations are required before a clear stall pattern can be recognised. The instantaneous variations of static pressure, and stall region at 70% height for the MS case, are shown in Figure 14. It is seen from this figure that a totally non-symmetric profile has developed for this case and the instantaneous variations of flow variables are totally different for each blade passage. Moreover, the fact that a gross amount of flow non-symmetry can be obtained with a very little amount of aerodynamic mistuning, lends support to the assumption that the final stall pattern is independent of the mistuning pattern. Furthermore, it is evident that the rotating stall creates a significant amount of unsteadiness. A matching between this unsteadiness and any of the assembly vibration modes is likely to result in very high response levels. It is also noticeable from Figure 14 that the rotating stall disturbances diffuse very rapidly downstream of Rotor 1, which is

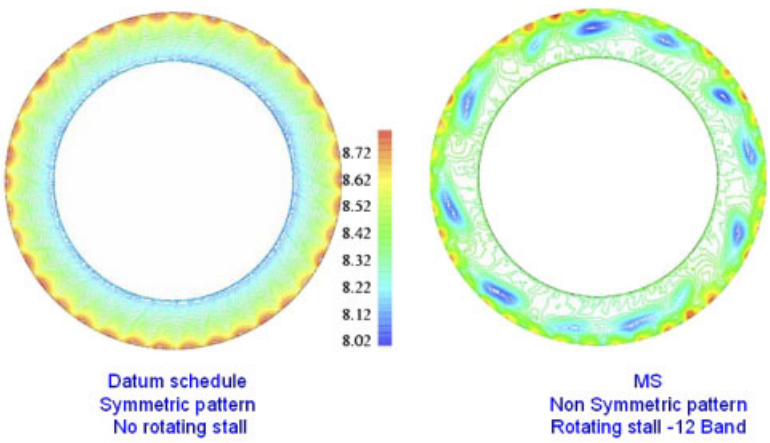

Figure 11. Instantaneous variations of static pressure upstream of Rotor 1.

DOI: 10.1002/fld

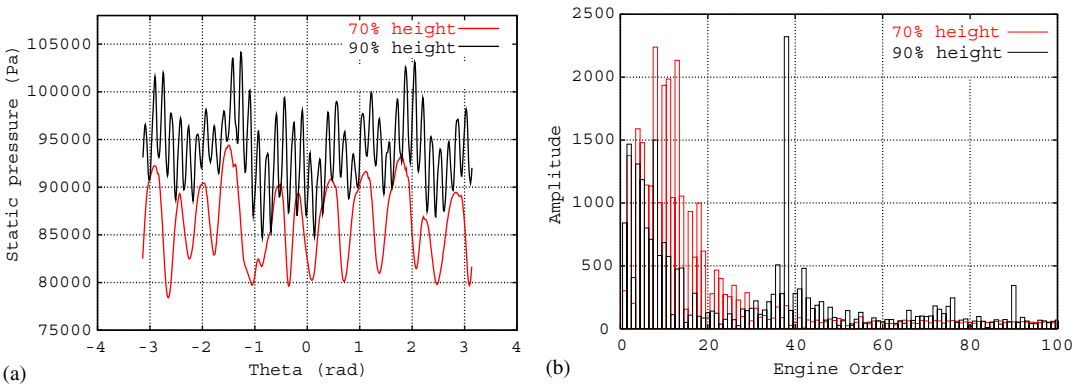

Figure 12. Variations of static pressure upstream of Rotor 1 and its Fourier components.

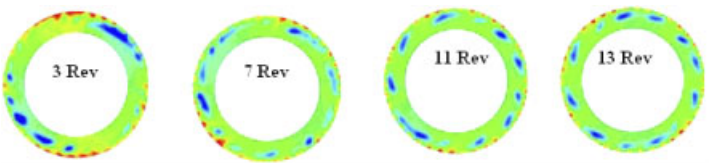

Figure 13. Time history of development of stall cell.

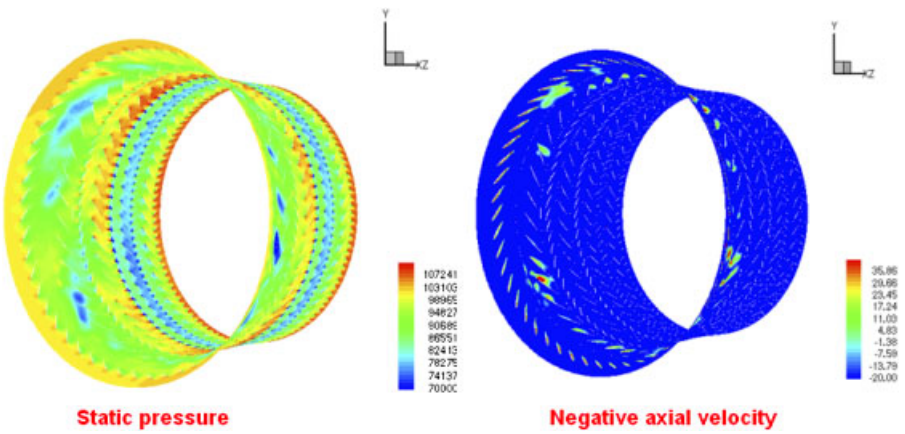

Figure 14. Instantaneous variations of static pressure and negative axial velocity at 70% height.

the only rotor that may suffer from excessive vibrations due to rotating stall. Such an observation is typical of high-band rotating stall behaviour where the unsteadiness remains confined to a single bladerow. This is further evident from Figure 15 which shows the Fourier components of rotating stall at successive planes, just upstream of the rotor bladerows. The disturbances diffuse very

DOI: 10.1002/fld

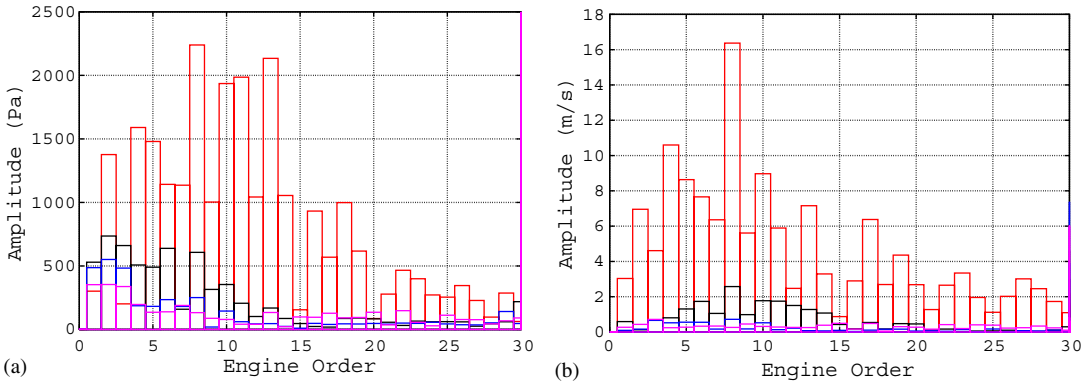

Figure 15. Fourier components of static pressure and axial velocity upstream of rotor blades.

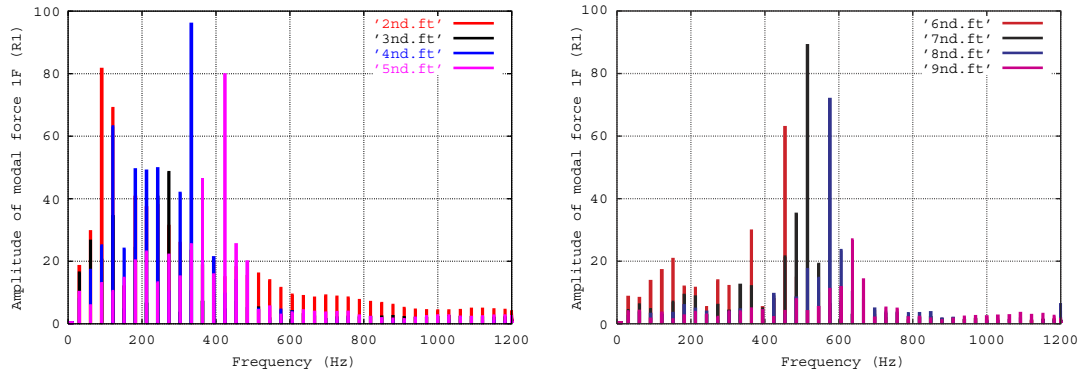

Figure 16. Fourier components of forcing on the blade.

rapidly and there is little evidence of rotating stall past Rotor 4. This finding suggests that similar results could have been obtained with a smaller model with fewer whole-annulus bladerows.

As mentioned earlier, the unsteadiness due to rotating stall interacts with the assembly vibration modes, a feature that creates unsteady forcing on the blade. The Fourier components of the unsteady forcing for different nodal diameter modes arising from the blade 1F mode are shown in Figure 16. In this case, the 1F natural frequency is 308 Hz and the 4ND forcing frequency is about 340 Hz. In the event of the two frequencies matching, the response in that mode is estimated to be about 20% of the chord using a Q-factor value of 200. The above results are in a very good agreement with engine data. The aerodynamic damping is likely to be very small during surge since there is no blade loading. The current method can automatically incorporate aero damping by virtue of calculating the pressure distribution provided that the blade motion is switched on. A fully coupled approach, where the blade motion is also taken into account, would be necessary if the unsteadiness created by the blade motion (and hence aero damping) was significant. However, such an approach would require many cycles before a limit cycle is reached and hence is, computationally, very expensive.

DOI: 10.1002/fld

6. CONCLUDING REMARKS

- The most important conclusion of this work is the feasibility of simulating rotating stall with a large-scale numerical model. Although the computational effort is significant, parallel processing on inexpensive PC clusters allows the runs to be undertaken in 'advanced design' timescales. For instance, the 9-bladerow model has about 60 million grid points and a typical run taking about 3 weeks on a 32-CPU cluster, each node consisting of a 2 GHz Intel Xeon CPU.
- From a numerical viewpoint, numerical stall initiation can be achieved by aerodynamically mistuning the rotor blade. Ideally, a systematic study needs to be undertaken to see if the obtained stall pattern and speed are independent of the initial stagger angle perturbation. Also, stall initiation is still relatively slow, requiring the simulation of about 13 full engine revolutions.
- In the present study the LP domain is placed upstream of the core compressor while a variable nozzle is placed downstream of the last compressor bladerow. With such an approach, it is not necessary to impose fixed stiff boundary conditions at the core compressor inlet or exit, and hence the unsteadiness is modelled naturally. Moreover, such an approach allows the modelling of LP/IP domain interactions which can be crucial in predicting the initiation of rotating stall.
- It is shown that the variable-vane scheduling plays an important role in determination of nature of rotating stall. From a steady-state flow point of view, the mal-scheduling results in a significant drop in flow, pressure ratio and efficiency.
- In the case of the high-band rotating stall predicted here, the disturbances diffuse very rapidly downstream. Hence, for such a case only Rotor 1 is likely to experience high response levels.
- From a design viewpoint, both the exact pattern and the speed of the rotating stall cells must be determined so that the critical vibration modes can be identified and avoided. However, such a requirement may not only be beyond the available modelling accuracy, but it also relies on both the pattern and speed to remain constant between successive rotations. The latter issue needs to be studied by undertaking long rotating stall simulations, say over 100 engine rotations, with representative inlet perturbations to see the stability or otherwise of the rotating stall structure.

ACKNOWLEDGEMENTS

The author would like to thank Rolls-Royce plc. for both sponsoring the work and allowing its publication. He also gratefully acknowledges the contributions of his Imperial College colleague Prof. M. Imregun and Mr G. Simpson of Rolls-Royce plc. in the form of many useful discussions.

REFERENCES

1. Greitzner EM. Surge and rotating stall in axial flow compressors. Parts 1 & 2. *Journal of Engineering for Power* (ASME) 1978; **98**:190–217.
2. Longley J, Hynes TP. Stability of flow through multi-stage axial compressors. *Journal of Turbomachinery* (ASME) 1990; **112**:126–132.
3. Weigl HJ, Paduano JD, Fréchette LG, Epstein AH, Greitzer EM, Bright MM, Strazisar AJ. Active stabilization of rotating stall and surge in a transonic single-stage compressor. *Journal of Turbomachinery* 1998; **120**:625–636.

DOI: 10.1002/fld

4. Moore F, Greitzer EM. A theory of post-stall transients in axial compressors. *Journal of Engineering for Gas Turbines and Power* (ASME) 1986; **108**:371–379.
5. Paduano J, Epstein AH, Greitzner EM, Guenette G. Modelling for control of rotating stall. *Automatica* 1994; **30**:1357–1373.
6. Niazi S. Numerical simulation of rotating stall and surge alleviation in axial compressors. *Ph.D. Thesis*, Georgia Institute of Technology, Department of Aerospace Engineering, Atlanta, U.S.A., 2000.
7. He L. Computational study of rotating stall inception in axial compressors. *AIAA Journal of Power and Propulsion* 1997; **13**(1):31–38.
8. Chen JP, Webster RS, Herrick GP, Hathaway MD, Skoch GJ. Numerical simulation of stall and stall control in axial and radial compressors. *AIAA-2006-0418*.
9. Spalart PR, Allmaras SR. A one-equation turbulence model for aerodynamic flows. *AIAA Paper 92-0439*, 1992.
10. Sayma AI, Vahdati M, Sbardella L, Imregun M. Modelling of 3D viscous compressible turbomachinery flows using unstructured hybrid grids. *AIAA Journal* 2000; **38**(6):945–954.
11. Sbardella L, Sayma A, Imregun M. Semi-structured meshes for axial turbomachinery blades. *International Journal for Numerical Methods in Fluids* 2000; **32**(5):569–584.
12. Rai MM. Implicit conservative zonal boundary scheme for Euler equation calculations. *Computers and Fluids* 1986; **14**:295–319.
13. Sayma AI, Vahdati M, Imregun M. Multi-bladerow fan forced response predictions using an integrated 3D time-domain aeroelasticity model. *Journal of Mechanical Engineering Science*, *Part C* 2000; **214**(12):1467–1483.
14. Vahdati M, Bréard C, Sayma A, Imregun M. An integrated time-domain aeroelasticity model for the prediction of fan forced response due to inlet distortion. *Journal of Engineering for Gas Turbines and Power* (ASME) 2003; **124**(1):196–208.
15. Vahdati M, Sayma A, Freeman C, Imregun M. On the use of atmospheric boundary conditions for axial-flow compressor stall simulations. *Journal of Turbomachinery* (ASME) 2005; **127**:349–351.

DOI: 10.1002/fld